ELSEVIER

Contents lists available at ScienceDirect

Materials Science in Semiconductor Processing

journal homepage: www.elsevier.com/locate/mssp





Grain orientation and transport properties of textured Bi₂Te₃ alloys

Oluwagbemiga P. Ojo a, Alan Thompson b, George S. Nolas a,*

- ^a Department of Physics, University of South Florida, Tampa, FL, 33620, USA
- b II-VI Incorporated, Dallas, TX, 75238, USA

ARTICLE INFO

Keywords:
Thermoelectric materials
Bismuth telluride alloys
Anisotropic transport properties
Crystallographic texture
X-ray diffraction
Rocking curve

ABSTRACT

The new material developments in the field of thermoelectrics over the past two decades have resulted in new materials with unique transport properties as well as new synthetic approaches. Enhanced thermoelectric properties of these new materials through thermal conductivity reduction and electrical properties enhancement strategies such as nano-structuring and band engineering have also been reported. Nevertheless, the material system upon which all new thermoelectric material developments are compared with continues to be alloys of Bi_2Te_3 . Approaches for thermoelectric property enhancements for Bi_2Te_3 alloys have also been undertaken, however, oriented polycrystalline materials continue to be of primary interest for thermoelectric device development. To this end we investigate n and p-type Bi_2Te_3 alloys provided by II-VI Inc. in order to elucidate the texturing in these materials and their transport properties with texturing. These materials are highly textured, as required in order to maximize the thermoelectric properties, with an 80% enhancement of the thermoelectric properties obtained with texturing.

1. Introduction

Thermoelectric devices provide solid-state thermal management and cooling as well as power generation from waste heat. Material developments continue to drive the research in the field, primarily in developing new materials with superior thermoelectric properties. The effectiveness of a material for thermoelectric applications is defined by the thermoelectric figure of merit $ZT = S^2 \sigma T / \kappa$, where *S* is the Seebeck coefficient, σ the electrical conductivity, κ the thermal conductivity and *T* the absolute temperature. Much of the effort over the last decade has focused on low thermal conductivity materials or optimized electrical properties [1–10]. Nevertheless, for thermoelectric devices bismuth telluride alloys continue to be the "gold standard" by which to judge other, new, material developments [11]. Bi₂Te₃ forms in the rhombohedral crystal structure, space group $R\overline{3}m$, with a relatively large c/alattice constant ratio and a layered structure that consist of -Te^[1]-Bi--Te^[2]-Bi-Te^[1]- layers with van der Waals bonds between adjacent Te layers [11-14], as shown in Fig. 1. This structure leads to anisotropy in the transport properties. However Bi₂Te₃-based alloys offer the most competitive advantage in both power factor ($S^2\sigma$) and ZT in the lower temperature regime (<450 K), including applications in micro and macro-scale waste heat recovery [15,16].

Along the a-b plane, the thermoelectric properties of Bi₂Te₃ alloys

are more favorable [11]. For example, for single crystal Bi₂Te₃ the ratio of the in-plane (the a-b plane) to the out-of-plane σ and κ is 5 and 2, respectively [17,18]. Large single crystals are readily grown; however, this will result in weak mechanical strength. Oriented polycrystalline bulk materials are therefore more desirable. Texture, or orientation of the grains, plays a key role in determining the optimized thermoelectric properties in polycrystalline Bi₂Te₃ alloy materials. Correlating the orientation distribution with thermoelectric transport properties is of interest and several studies have, even recently, been undertaken on melt-grown [19], ball-milled and densified [20-23], and extruded [24-27] materials. In addition, thermoelectric properties optimization with texturing of other thermoelectric materials are ongoing [28–30]. Nevertheless, investigations into materials currently in use in devices are rare. Moreover, quantitative investigations of texturing both perpendicular and parallel to the growth direction are not typically undertaken. Herein we report on the effect of texturing on the transport properties of materials from II-VI Inc., polycrystalline *n*-type Bi₂Te_{2.7}Se_{0.3} and p-type Bi_{0.5}Sb_{1.5}Te₃, synthesized from the melt [11, 31]. The quality of crystallographic orientation was investigated employing an approach that quantifies texture quality by X-ray diffraction (XRD) and rocking curve (RC) analyses [32,33]. In-plane σ , S, κ and ZT data are compared with that of out-of-plane in order to correlate texturing with transport and thermoelectric properties.

E-mail address: gnolas@usf.edu (G.S. Nolas).

 $^{^{\}ast}$ Corresponding author.

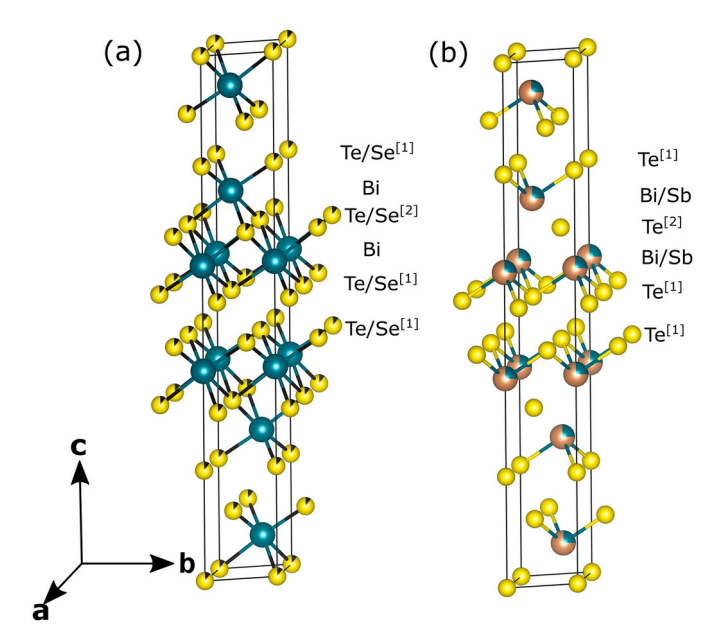


Fig. 1. The crystal structure of (a) $Bi_2Te_{2.7}Se_{0.3}$ with the Bi atoms represented by green circles at the 6c crystallographic site, and $Te/Se^{[1]}$ and $Te/Se^{[2]}$ atoms represented by yellow/black circles at the 6c and 3a crystallographic sites, respectively, and (b) $Bi_{0.5}Sb_{1.5}Te_3$ with the Bi/Sb atoms represented by blue/brown circles at the 6c crystallographic site, and the $Te^{[1]}$ and $Te^{[2]}$ atoms represented by yellow circles at the 6c and 3a crystallographic sites, respectively.

2. Experimental

The *n*-type Bi₂Te_{2.7}Se_{0.3} and *p*-type Bi_{0.5}Sb_{1.5}Te₃ were prepared from the melt in a similar manner as reported elsewhere [11,31]. The ingots were cut using a wire saw into parallelepipeds and the surfaces were polished to a fine surface finish for XRD analyses. XRD data were collected with a Bruker-AXS D8 Focus diffractometer in Bragg-Brentano geometry with a Cu K_{α} radiation and a graphite monochromator. As shown in Fig. 2, XRD data from the longitudinal sections were collected from parallelepiped sections, where the surface is parallel to the ingot growth direction, and XRD from the transverse sections were collected perpendicular to the ingot growth direction. XRD scans were collected twice from each surface by rotating the specimens 180°, which we will refer to as an in-plane rotation φ . XRD θ -2 θ scans were collected using a 1 mm incident slit size and ω -scans (RC) were collected using 0.6 mm and 0.225 mm incident and collecting slit sizes, respectively. The Lotgering orientation factor, F, [34], was calculated from XRD θ -2 θ data. Optical micrographs were obtained on polished surfaces using a Nikon

Metallographic optical microscope. The transport properties were measured using a modified Harmon technique [35].

3. Results and discussion

Fig. 3 shows representative optical micrographs on polished surfaces of the grain morphology parallel and perpendicular to the ingot growth directions for the n and p-type materials. Strong grain alignment is observed from micrographs of surfaces perpendicular to the ingot growth direction, as shown in Fig. 3(b) and (d), while the size of the plate-like grains is evident along the growth direction in Fig. 3(a) and (c). In addition to grain orientation, grain size, morphology, and tilt, relative to the Bragg angle of interest, will influence the XRD RC data, described below, and one reason why XRD analyses are typically undertaken along $\{00l\}$ planes (i.e. perpendicular to the growth direction) on such melt-grown materials.

Fig. 4(a) and (b) show XRD data of the longitudinal section of n and p-type $\mathrm{Bi}_2\mathrm{Te}_3$ alloy materials, respectively. The powder XRD patterns were indexed to the rhombohedral crystal structure type with space group $R\overline{3}m$ [13]. As shown in Fig. 4, the intensity of the (00l) peaks were much larger as compared to that of the powder pattern. This clearly indicates preferred orientation of the (00l) planes perpendicular to the ingot growth direction for both the n-type and p-type specimens. The Lotgering value, F, for diffraction peaks between 15° and 70° were calculated using

$$F = \frac{P - P_o}{1 - P_o} \tag{1}$$

where $P_o = \sum I_0(00l)/\sum I_o(hkl)$, $P = \sum I(00l)/\sum I(hkl)$, and I and I_0 are the peak integrated intensities for the textured and randomly oriented specimen, respectively. Other preferred orientation directions can be analyzed by replacing (00l) with the corresponding planes. An F value of zero indicates that grains are randomly oriented, whereas an F value of 1.0 indicates a perfect orientation of all grains. In our analyses, F is 0.98 and 0.81 for the n-type and p-type specimens, respectively, indicated strong texturing of the basal planes when the normal to the (00l) basal planes are perpendicular to the ingot growth direction as illustrated in Fig. 2(b). It is important to note that the observed relative peak intensity of the θ -2 θ XRD pattern of the longitudinal sections depend on how the specimen was cut. This may result in relative misalignment that may lead to an underestimation of F [36]. XRD RC (ω -scan) was therefore employed in order to overcome any potential misalignment issues from sample preparation.

Fig. 5(a) and (b) show the XRD RC data for (00.15) ($2\theta=44.8^{\circ}$ and 44.6° for the n and p-type specimens, respectively) from a longitudinal section of the specimens. The RC data from several different pieces resulted in full width at half maximum (FWHM) values of 0.67° and 1.3° for the n-type and p-type specimens, respectively, indicating strong

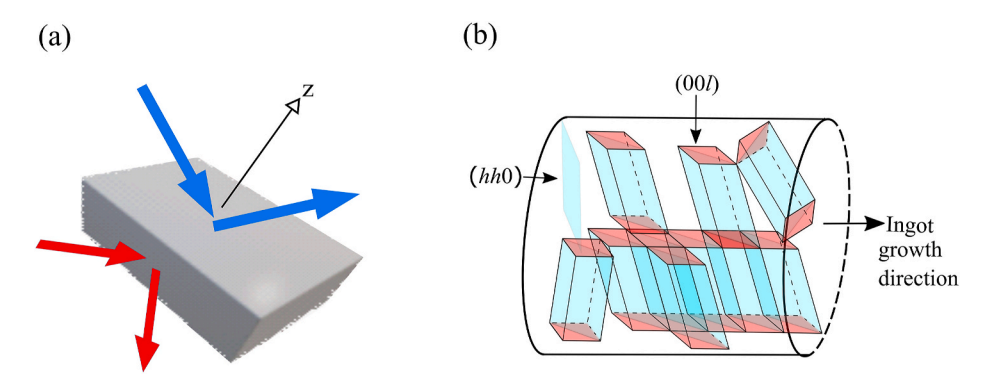


Fig. 2. Schematics illustrating (a) the two surfaces employed in this study, where red arrows show the longitudinal section, blue arrows show the transverse section and z is the ingot growth direction, and (b) the (00l) and the (hh0), e.g. (110), planes perpendicular and parallel to the ingot growth direction, respectively. The color is intended as an indication of the particular surface investigated.

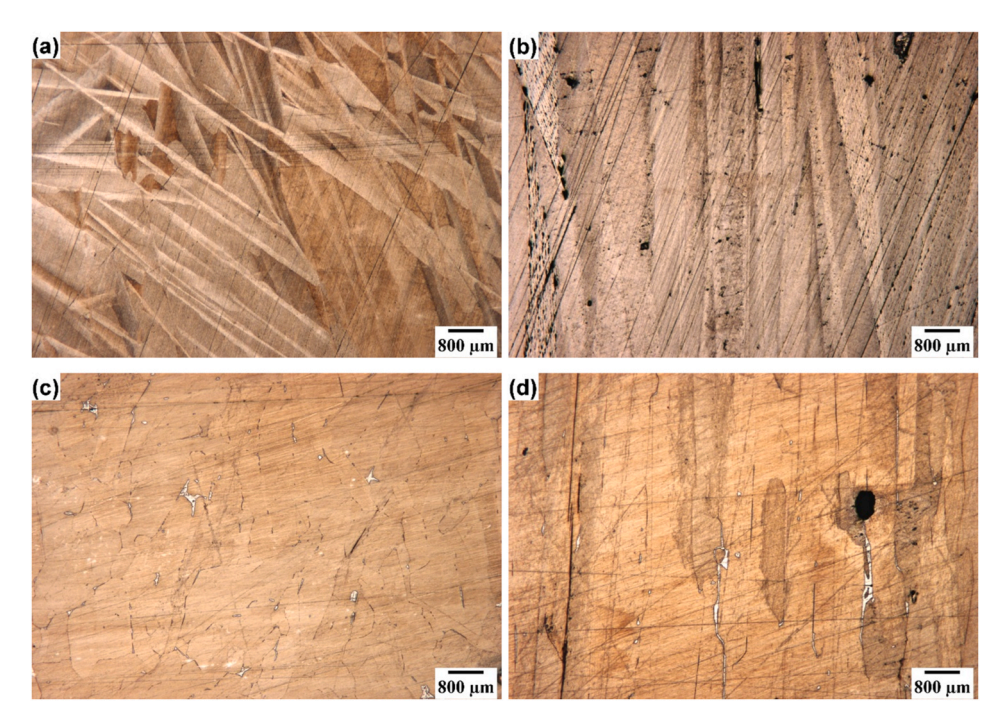


Fig. 3. Optical micrographs of n-type Bi₂Te_{2.7}Se_{0.3} taken (a) parallel to the ingot growth direction and (b) perpendicular to the ingot growth direction, and p-type Bi_{0.5}Sb_{1.5}Te₃ taken (c) parallel to the ingot growth direction and (d) perpendicular to the ingot growth direction.

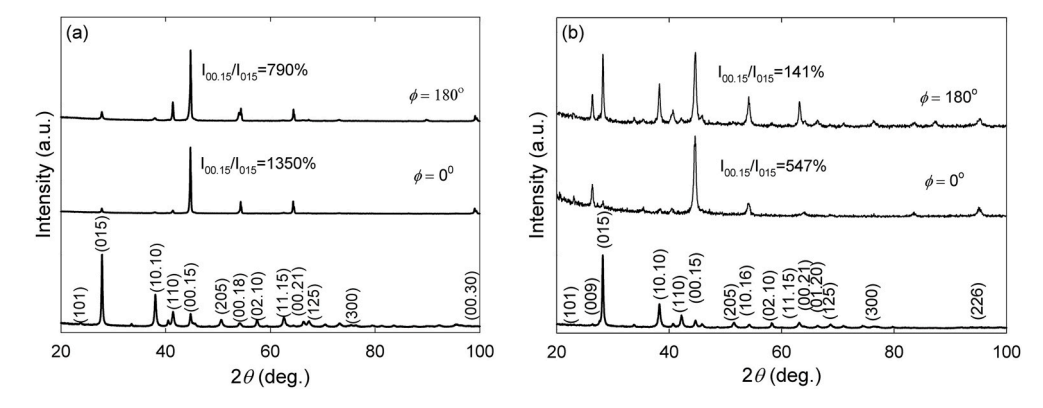


Fig. 4. XRD data for (a) n-type Bi₂Te_{2.7}Se_{0.3} for powder (bottom) and a longitudinal section of the specimen at 0° (middle) and 180° (top) in-plane rotation of the specimen, with F values of 0.98 and 0.91, respectively, and (b) p-type Bi_{0.5}Sb_{1.5}Te₃ powder (bottom) and a longitudinal section of the specimen at 0° (middle) and 180° (top) in-plane rotation of the specimen, with F values of 0.81 and 0.60, respectively.

texturing along the (00*l*) basal planes for both the *n*-type and *p*-type specimens. In fact, the FWHM values are close to that of high quality single crystals [37]. Very strong texturing for Bi₂Te₃ alloys is crucial as σ , in particular, decreases rapidly with unfavorable orientation [11,17, 19,20,22,38]. For further comparison, for the case of random grain orientation obtained by grinding a piece of the material to fine powder, a near constant intensity level for the XRD RC is expected [32,33,39], as shown in Fig. 6 for Bi₂Te_{2.7}Se_{0.3} as an example. We note that the shift in the RC maximum, as shown in Fig. 5, is primarily due to deviation of the texture axis from the specimen normal. The wing peak, [40], as shown in Fig. 5(a) for $\varphi = 0^{\circ}$ and 180° , is due to a small angle tilt misorientation of about 1.5°, potentially from preparation of the different sections as described above.

Strong texture of the basal planes does not typically imply equally significant texture for other planes. In fact, analyses similar to that described above are typically *not done* for the {110} planes (planes perpendicular to 00*l*) due to weak preferred orientation along these planes despite the fact that strong texturing occurs along the basal planes [41,42]. Nevertheless, it is instructive to analyze (110) for

completeness and, as described below, we observe texturing in this orientation for these materials as well. Fig. 7 shows the data and results of the transverse section (see Fig. 2(a)) for the n and p-type specimens. From the XRD data, shown in Fig. 7(a) and (b), F is 0.45 and 0.14 for the n and p-type specimens, respectively. These data indicate the n-type material is well oriented along (110). This type of analysis is rare, yet important as the thermoelectric properties of polycrystalline Bi₂Te₃ alloys is very closely related to the degree of texturing. Furthermore, the F values from our XRD data from the transverse sections of specimens indicated orientation of other diffracting planes (e.g. (015) and (300) with F = 0.26 and 0.10, respectively) for the p-type specimen. This implies competing anisotropic grain orientation in the transverse direction. It should be noted that for optimal comparison for these F calculations, PowderCell software was used to simulate randomly oriented XRD patterns for both n and p-type compositions as a small amount of preferred orientation was observed even for powder XRD data. This is typical for materials with layered crystal structures. Furthermore, during the RC measurements the lattice planes of one type (i.e. the same d-spacing) were probed via the detector set at the Bragg angle (2heta =

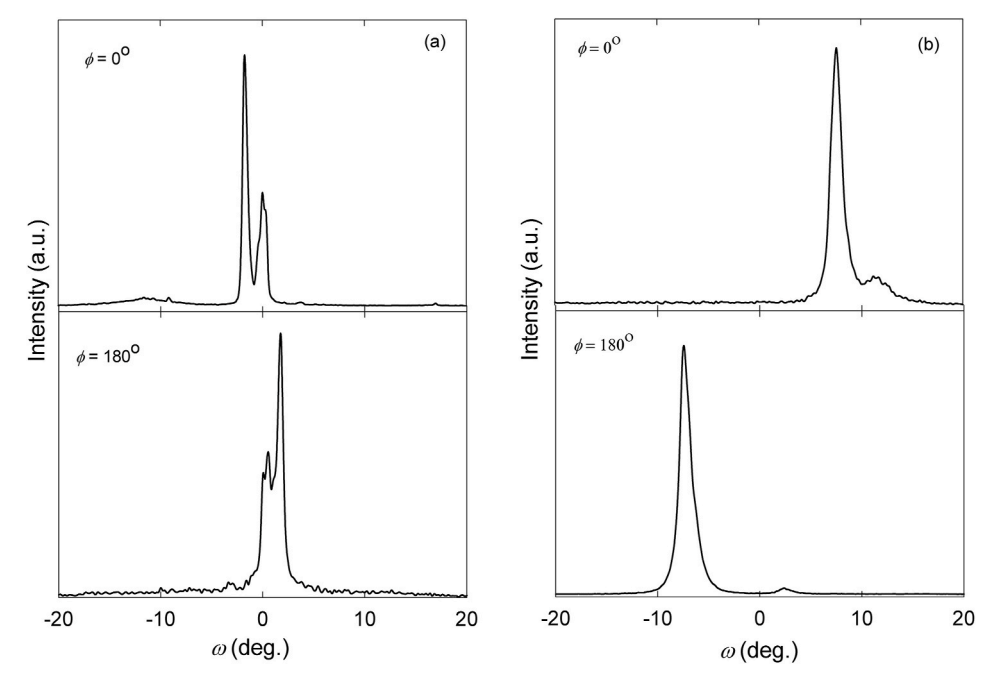


Fig. 5. XRD RC of (00.15) from a longitudinal section of (a) n-type $Bi_2Te_{2.7}Se_{0.3}$ at 0° and 180° in-plane rotation of the specimen, and (b) p-type $Bi_{0.5}Sb_{1.5}Te_3$ at 0° and 180° in-plane rotation of the specimen.

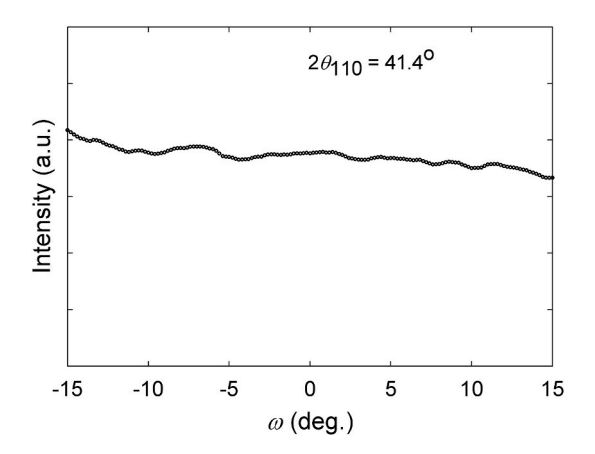


Fig. 6. XRD RC of powder $Bi_2Te_{2.7}Se_{0.3}$ showing near-constant intensity, as expected for random orientation of the grains.

41.4° and 42.2° for the n and p-type specimens, respectively) while the specimen was tilted. The intensity recorded corresponds to grains with {110} planes perpendicular to the diffraction vector in the Bragg Brentano geometry and those within some maximum angular deviation that depends on certain geometrical characteristics of the diffractometer [43]. The FWHM of a RC is therefore a measure of the quality of orientation, as described above for the case of the basal planes. We again note FWHM values for (110) in investigations of Bi_2Te_3 alloys are not typically reported due to multiple peaks; however, the RC data reflects the average orientational distribution of the grains [44], as shown in Fig. 7.

The transport properties of the n and p-type materials were investigated in order to clearly illustrate the influence of grain orientation on the transport properties. Fig. 8 shows the temperature-dependent transport properties along the a-b plane, i.e. measured in the ingot growth direction. In comparison with ball-milled and hot-pressed materials with similar compositions, κ is marginally higher however the power factor is nearly twice as high thereby resulting in superior ZT values [45,46]. In order to further quantify directional enhancement,

room temperature transport properties perpendicular to the a-b plane were also measured with the results shown in Table 1. The data clearly demonstrate the impact orientation has on the transport properties, particularly for σ . Unlike σ and κ , there is no significant difference in S with direction, as reported for Bi₂Te₃ [47]. The impact on σ is partly due to charge mobility that is high along the growth direction relative to the perpendicular direction [48]. Thus for bismuth telluride alloys with transport properties that vary with crystallographic direction, strong texturing is required for optimum thermoelectric performance.

4. Conclusions

For the purpose of elucidating the degree of texturing in materials that are currently in use in thermoelectric devices, and to investigate their texture-transport property relationships, XRD and transport data along the longitudinal and transverse sections of n and p-type $\mathrm{Bi}_2\mathrm{Te}_3$ alloys were investigated. The basal planes were preferentially oriented perpendicular, and the $\{110\}$ planes were preferentially oriented parallel, to the ingot growth direction. High orientation factor and small RC FWHM were observed, which lead to the observed strong thermoelectric properties. Large enhancement in ZT is obtained along the ingot direction relative to the perpendicular direction, largely due to the anisotropy in σ . Enhanced thermoelectric properties for polycrystalline bismuth telluride alloys, as well as other anisotropic thermoelectric materials, will necessarily require strong grain texturing regardless of doping or other enhancement strategies.

CRediT authorship contribution statement

Oluwagbemiga P. Ojo: Data curation, Formal analysis, Visualization. **Alan Thompson:** Conceptualization, Data curation. **George S. Nolas:** Conceptualization, Writing – original draft, Writing – review & editing, Supervision, Funding acquisition.

Declaration of competing interest

The authors declare that they have no known competing financial interests or personal relationships that could have appeared to influence

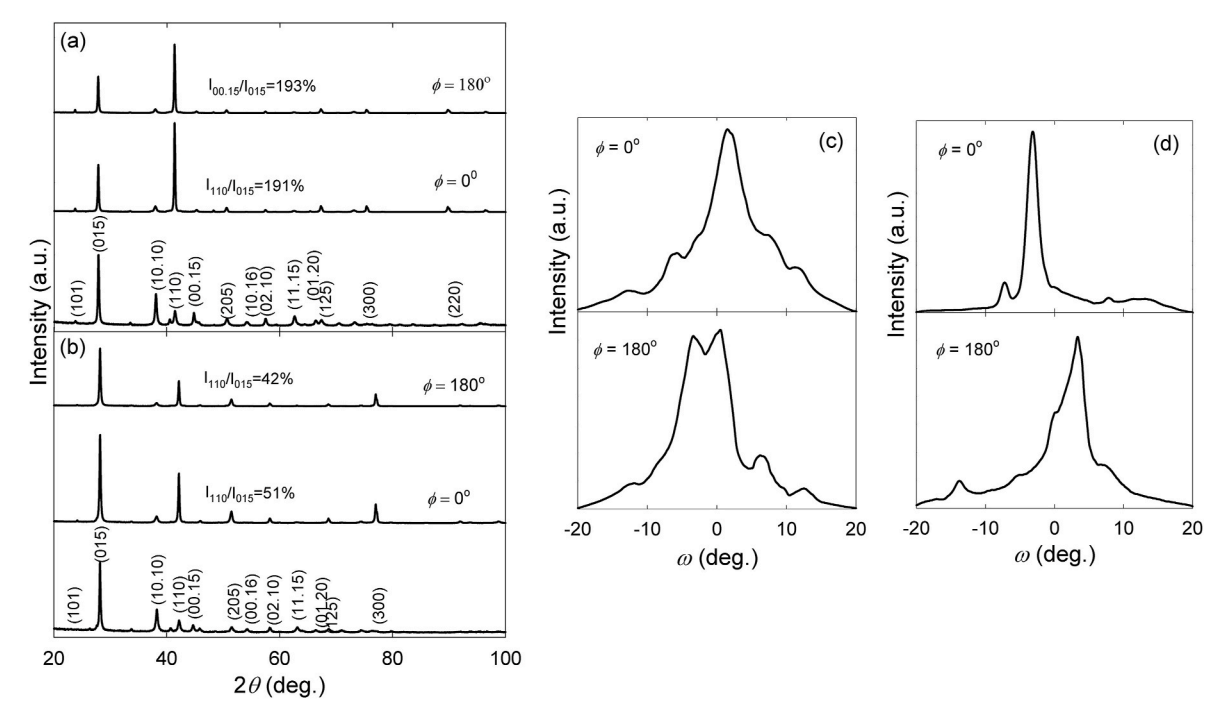


Fig. 7. (a) Powder XRD data (bottom) of n-type Bi $_2$ Te $_2$, $_7$ Se $_{0.3}$ in comparison to data from a transverse section of the specimens at 0° (middle) and 180° (top) in-plane rotation of the specimen, with F values of 0.45 and 0.38, respectively, (b) powder XRD data (bottom) for p-type Bi $_0.5$ Sb $_1.5$ Te $_3$ in comparison to data from a transverse section of the specimen at 0° (middle) and 180° (top) in-plane rotation of the specimen, with F values of 0.14 and 0.05, respectively, (c) XRD RC of (110) from a transverse section of p-type Bi $_0.5$ Sb $_1.5$ Te $_3$ at 0° and 180° in-plane rotation of the specimen, and (d) XRD RC of (110) from a transverse section of p-type Bi $_0.5$ Sb $_1.5$ Te $_3$ at 0° and 180° in-plane rotation of the specimen.

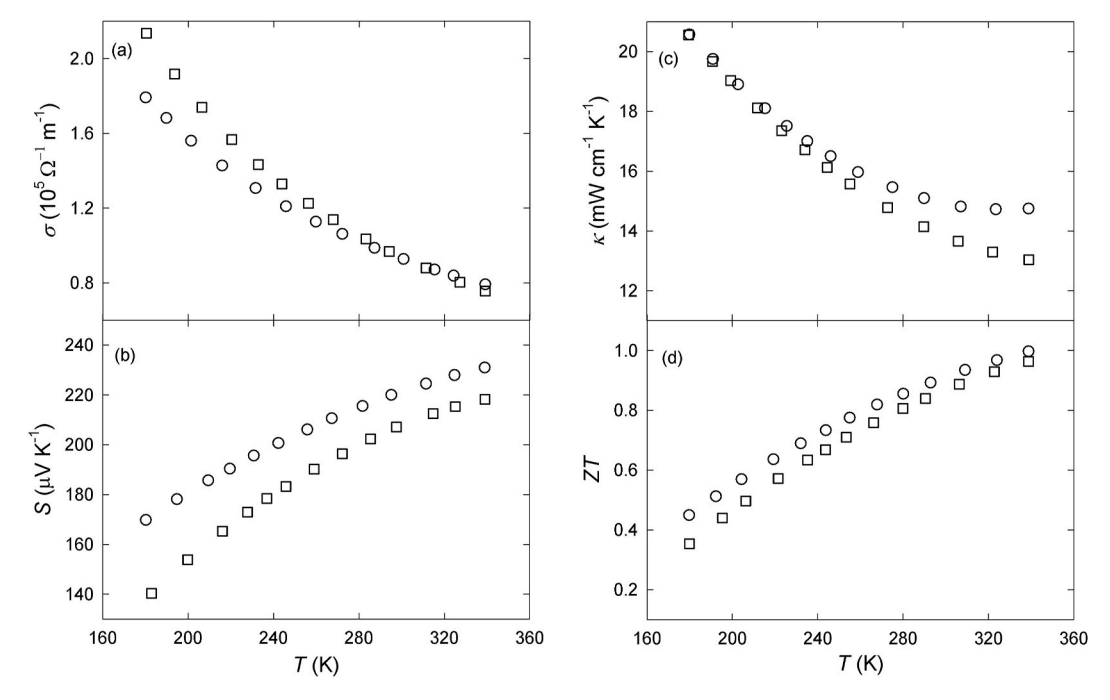


Fig. 8. Temperature dependent (a) ρ , (b) modulus of S, (c) κ and (d) ZT of n-type $Bi_2Te_{2.7}Se_{0.3}$ (circles) and p-type $Bi_{0.5}Sb_{1.5}Te_3$ (squares) as measured parallel to the a-b plane.

Table 1

The ratio of room temperature transport properties of n-type $Bi_2Te_{2.7}Se_{0.3}$ and p-type $Bi_0.5Sb_{1.5}Te_3$ measured along and perpendicular to the ingot growth directions. The symbol \parallel (parallel) and \perp (perpendicular) refer to the ingot growth direction.

	<i>n</i> -type	<i>p</i> -type
$\sigma_\parallel/~\sigma_\perp$	2.1	2.6
$egin{aligned} \sigma_{\parallel}/\ \sigma_{\perp} \ & \ S_{\parallel}/\ S_{\perp} \ & \ \kappa_{\parallel}/\ \kappa_{\perp} \end{aligned}$	1.0	1.0
$\kappa_{\parallel}/\ \kappa_{\perp}$	1.3	1.4
$ZT_{\parallel}/$	1.6	1.8
$ZT_{\perp}{ m v}$		

the work reported in this paper.

Acknowledgements

This work was supported by the National Science Foundation, Grant No. DMR-1748188. O.P. acknowledges support from the II-VI Foundation Block-Gift Program.

References

- M. Beekman, D.T. Morelli, G.S. Nolas, Nat. Mater. 14 (2015) 1182, https://doi.org/ 10.1038/nmat4461
- [2] K. Biswas, J. He, I.D. Blum, C.I. Wu, T.P. Hogan, D.N. Seidman, V.P. Dravid, M. G. Kanatzidis, Nature 489 (2012) 414, https://doi.org/10.1038/nature11439.
- [3] G.S. Nolas, G.A. Slack, Am. Sci. 89 (2001) 136.
- [4] A. Datta, J. Paul, A. Kar, A. Patra, Z. Sun, L. Chen, J. Martin, G.S. Nolas, Cryst. Growth Des. 10 (2010) 3983, https://doi.org/10.1021/cg100560s.
- [5] J. Xin, Y. Tang, Y. Liu, X. Zhao, H. Pan, T. Zhu, npj Quant Mater 3 (2018) 9, https://doi.org/10.1038/s41535-018-0083-6.
- [6] P. Sundarraj, D. Maity, S.S. Roy, R.A. Taylor, RSC Adv. 4 (2014) 46860, https://doi.org/10.1039/C4RA05322B.
- [7] P. Gorai, V. Stevanović, E.S. Toberer, Nat. Rev. Mater. 2 (2017) 17053, https://doi. org/10.1038/natreymats.2017.53.
- [8] M.S. Dresselhaus, G. Chen, M.Y. Tang, R.G. Yang, H. Lee, D.Z. Wang, Z.F. Ren, J. P. Fleurial, P. Gogna, Adv. Mater. 19 (2007) 1043, https://doi.org/10.1002/ADMA.200600527.
- [9] G.S. Nolas, H.J. Goldsmid, Phys. Status Solidi 194 (2002) 271.
- [10] G. Tan, F. Shi, S. Hao, H. Chi, T.P. Bailey, L.D. Zhao, C. Uher, C. Wolverton, V. P. Dravid, M.G. Kanatzidis, J. Am. Chem. Soc. 137 (2015) 11507, https://doi.org/10.1021/jacs.5b07284.
- [11] G.S. Nolas, J. Sharp, J. Goldsmid, Thermoelectrics Basic Principles and New Materials Developments, Springer, New York, 2001, pp. 111–145, and references therein.
- [12] I.T. Witting, F. Ricci, T.C. Chasapis, G. Hautier, G.J. Snyder, Research 2020 (2020) 4361703, https://doi.org/10.34133/2020/4361703.
- [13] S. Nakajima, J. Phys. Chem. Solid. 24 (1963) 479, https://doi.org/10.1016/0022-3697(63)90207-5.
- [14] I.J. Ohsugi, T. Kojima, I.A. Nishida, J. Appl. Phys. 68 (1990) 5692, https://doi.org/ 10.1063/1.346985.
- [15] B.I. Ismail, W.H. Ahmed, Recent pat. Electr. Electron. Eng. 2 (2009) 27, https://doi.org/10.2174/1874476110902010027.
- [16] H.J. Goldsmid, Materials 7 (2014) 2577, https://doi.org/10.3390/ma7042577.
- [17] A. Jacquot, N. Farag, M. Jaegle, M. Bobeth, J. Schmidt, D. Ebling, H. Böttner, J. Electron. Mater. 39 (2010) 1861, https://doi.org/10.1007/s11664-009-1059-x.

- [18] S. Kudo, S. Tanaka, K. Miyazaki, Y. Nishi, M. Takashiri, Mater. Trans. 58 (2017) 513, https://doi.org/10.2320/matertrans.M2016295.
- [19] L. Hu, H. Wu, T. Zhu, C. Fu, J. He, P. Ying, X. Zhao, Adv. Energy Mater. 5 (2015) 1500411, https://doi.org/10.1002/aenm.201500411.
- [20] H. Kitagawa, A. Kurata, H. Araki, S. Morito, E. Tanabe, J. Electron. Mater. 39 (2010) 1692, https://doi.org/10.1007/s11664-010-1181-9.
- [21] Z. Zhang, P.A. Sharma, E.J. Lavernia, N. Yang, J. Mater. Res. 26 (2011) 475, https://doi.org/10.1557/jmr.2010.67.
- [22] L.D. Zhao, B.P. Zhang, J.F. Li, H.L. Zhang, W.S. Liu, Solid State Sci. 10 (2008) 651, https://doi.org/10.1016/i.solidstatesciences.2007.10.022.
- [23] Q. Lognoné, F. Gascoin, O.I. Lebedev, L. Lutterotti, S. Gascoin, D. Chateigner, J. Am. Ceram. Soc. 97 (2014) 2038, https://doi.org/10.1111/jace.12970.
- [24] R. Srinivasan, N. Gothard, J. Spowart, Mater. Lett. 64 (2010) 1772, https://doi. org/10.1016/j.matlet.2010.05.018.
- [25] S. Miura, Y. Sato, K. Fukuda, K. Nishimura, K. Ikeda, Mat. Sci. Eng.: A 277 (2000) 244, https://doi.org/10.1016/S0921-5093(99)00539-0.
- T. Hayashi, M. Sekine, J. Suzuki, Y. Horio, Mater. Trans. 47 (2006) 1941, https://doi.org/10.2320/matertrans.47.1941.
- [27] Z.L. Wang, K. Matsuoka, T. Araki, T. Akao, T. Onda, Z.C. Chen, Procedia Eng 81 (2014) 616, https://doi.org/10.1016/j.proeng.2014.10.049.
- [28] P.P. Shang, J. Dong, J. Pei, F.H. Sun, Y. Pan, H. Tang, B.P. Zhang, L.D. Zhao, J.F. Li, Research (2019) 1, https://doi.org/10.34133/2019/9253132, 2019.
- [29] D. Kenfaui, M. Gomina, J. Noudem, D. Chateigner, Materials 11 (2018) 1224, https://doi.org/10.3390/ma11071224.
- [30] Y. Luo, C. Du, Q. Liang, Y. Zheng, B. Zhu, H. Hu, K.A. Khor, J. Xu, Q. Yan, M. G. Kanatzidis, Small 14 (2018) 1803092, https://doi.org/10.1002/smll.201803092.
- [31] H.J. Goldsmid, Recent Trends in Thermoelectric Materials Research I, in: T.M. Tritt (Ed.), Academic Press, 2001, pp. 13–14.
- [32] M.D. Vaudin, M.W. Rupich, M. Jowett, G.N. Riley, J.F. Bingert, J. Mater. Res. 13 (1998) 2910, https://doi.org/10.1557/JMR.1998.0398.
- [33] C.Z. Yuan, Z.W. Min, L. Jiang, Mater. Struct. 21 (1988) 329, https://doi.org/ 10.1007/BF02472158.
- [34] F.K. Lotgering, J. Inorg. Nucl. Chem. 9 (1959) 113, https://doi.org/10.1016/0022-
- [35] T.C. Harman, J. Appl. Phys. 29 (1958) 1373, https://doi.org/10.1063/1.1723445.
- [36] S. Grasso, N. Tsujii, Q. Jiang, J. Khaliq, S. Maruyama, M. Miranda, K. Simpson, T. Mori, M.J. Reece, J. Mater. Chem. C 1 (2013) 2362, https://doi.org/10.1039/ C3TC30152D.
- [37] D. Joseph Daniel, A. Raja, J.Y. Lee, D. Balaji, H.J. Kim, P. Ramasamy, CrystEngComm 20 (2018) 4989, https://doi.org/10.1039/C8CE00772/
- [38] T. Caillat, M. Carle, P. Pierrat, H. Scherrer, S. Scherrer, J. Phys. Chem. Solid. 53 (1992) 1121, https://doi.org/10.1016/0022-3697(92)90087-T.
- [39] G. Zilahi, T. Ungár, G. Tichy, J. Appl. Crystallogr. 48 (2015) 418, https://doi.org/ 10.1107/\$1600576715001466.
- [40] P. Mikulík, D. Lübbert, P. Pernot, L. Helfen, T. Baumbach, Appl. Surf. Sci. 253 (2006) 188, https://doi.org/10.1016/j.apsusc.2006.05.084.
- [41] M. Ashida, T. Hamachiyo, K. Hasezaki, H. Matsunoshita, M. Kai, Z. Horita, J. Phys. Chem. Solid. 70 (2009) 1089, https://doi.org/10.1016/j.jpcs.2009.06.002.
- [42] K. Hasezaki, Y. Morisaki, H. Araki, H. Kitagawa, E. Tanabe, Mater. Trans. 47 (2006) 383, https://doi.org/10.2320/matertrans.47.383.
- [43] P. Andonov, J. Appl. Crystallogr. 24 (1991) 355, https://doi.org/10.1107/ S0021889891002820.
- [44] J.E. Blendell, M.D. Vaudin, E.R. Fuller, J. Am. Ceram. Soc. 82 (2004) 3217.
- [45] X. Yan, B. Poudel, Y. Ma, W.S. Liu, G. Joshi, H. Wang, Y. Lan, D. Wang, G. Chen, Z. F. Ren, Nano Lett. 10 (2010) 3373, https://doi.org/10.1021/nl101156v.
- [46] H. Kitagawa, A. Kurata, H. Araki, S. Morito, E. Tanabe, J. Electron. Mater. 39 (2010) 1692, https://doi.org/10.1007/s11664-010-1181-9.
- [47] J.H. Dennis, Adv. Energy Convers. 1 (1961) 99, https://doi.org/10.1016/0365-1789(61)90012-1.
- [48] P.H. Egli (Ed.), Thermoelectricity: Including the Proceedings of the Conference on Thermoelectricity, Wiley, 1960, pp. 109–120.